

# Verification of the elasto-plastic behavior of nonlinear concrete material models

Petr Kral, Jiri Kala, and Petr Hradil

**Abstract**—The aim of this paper is the verification of the behavior of nonlinear concrete material models subjected to dynamic loading. The behavior of five selected nonlinear concrete models is tested within numerical simulations of the testing of the mechanico-physical properties of concrete in uniaxial and triaxial compression, using cylinders. These numerical simulations are performed using the explicit finite element approach and their results take the form of load-displacement and load-time diagrams created for a concrete cylinder under dynamic compressive loading whose behavior was calculated by individual nonlinear models of concrete. The results gained from the numerical simulations are compared with experimental results obtained from laboratory tests performed for the purpose of verifying the nonlinear concrete models. This comparison shows the differences in the behavior of the individual nonlinear models of concrete and the approximations of the experimental data. The comparison allows conclusions to be drawn as to which nonlinear models provide the best approximation of the test data, and therefore which models best describe the behavior of the tested concrete in compression.

**Keywords**—Dynamic compressive loading, experiment, finite element simulation, LS-DYNA software, nonlinear concrete material model.

## I. INTRODUCTION

THE numerical modeling of structures or their components with the aim of investigating their behavior with the aid of computational systems based on the finite element method is a commonly used procedure during the design of structures or structural elements. Current innovative finite element procedures (implicit, explicit or combined solvers) offer an inexhaustible amount of material models. These material models are usually linear, bilinear or multilinear, but can also be strongly nonlinear. Nonlinear material models undoubtedly have their place in sophisticated analysis and for this reason it

This paper was created with the financial support of project GACR 14-25320S “Aspects of the use of complex nonlinear material models” provided by the Czech Science Foundation and under the project No. LO1408 “AdMaS UP - Advanced Materials, Structures and Technologies”, supported by Ministry of Education, Youth and Sports under the „National Sustainability Programme P”.

Petr Kral is with the Institute of Structural Mechanics, Faculty of Civil Engineering, Brno University of Technology, Veveri 331/95, 602 00 Brno, Czech Republic (e-mail: kral.p@fce.vutbr.cz).

Jiri Kala is with the Institute of Structural Mechanics, Faculty of Civil Engineering, Brno University of Technology, Veveri 331/95, 602 00 Brno, Czech Republic (e-mail: kala.j@fce.vutbr.cz).

Petr Hradil is with the Institute of Structural Mechanics, Faculty of Civil Engineering, Brno University of Technology, Veveri 331/95, 602 00 Brno, Czech Republic (e-mail: hradil.p@fce.vutbr.cz).

is appropriate to test and validate them with the aim of achieving their optimal function.

A number of publications have been dedicated to the nonlinear modeling of concrete, e.g. [1]–[8]. Worldwide, nonlinear material models of concrete are most often used for the numerical modeling of concrete structures subjected to specific loading during which the effect of the strain rate upon the mechanico-physical properties of concrete is apparent. Information regarding nonlinear models of concrete and results obtained from various numerical simulations in which nonlinear models of concrete were used, and in which strain rate played an important role, can be found in the literature: see the references section for examples [9]–[16].

This paper details the subsection of five different nonlinear material models of concrete to dynamic compressive loading. The behavior of the selected models was tested within the context of numerical simulations of the testing of the mechanico-physical properties of concrete in uniaxial and triaxial compression, using cylinders. The results gained from the numerical simulations take the form of load-displacement and load-time diagrams for a concrete cylinder whose behavior was calculated by individual nonlinear concrete models. These diagrams were analyzed. They show the differences in concrete behavior for the individual nonlinear models. The results gained from the numerical simulations are compared with experimental data obtained from laboratory tests.

## II. EXPERIMENTS

Experiments were carried out in order to compare their results within this paper with the results obtained from the aforementioned numerical simulations. On the basis of this comparison the behavior of the nonlinear concrete models can be verified.

### A. Outline of the experiments

Each experiment involved testing the mechanico-physical properties of concrete cylinders subjected to uniaxial compression.

The tests were carried out on three identical cylindrical concrete specimens with a height of approx. 305 mm and a base diameter of approx. 152 mm. The specimens were placed between steel plates and a strain gauge was installed in the middle of each of them (see Fig. 1). The mean value of the ultimate concrete strength in uniaxial compression varied around 43 MPa.



Fig. 1 Concrete cylinder between steel plates

The specimens were compressed at a constant velocity of approx. 1.27 mm/s and the test duration, strain deformation, relative vertical displacement and compressive force exerted by the test apparatus were monitored during the tests.

### B. Experimental results

The results gained from the experiments conducted on cylindrical specimens in uniaxial compression are depicted in a load-time diagram (see Fig. 2). With regard to the fact that the relationship between the displacement of the cylinder base and time is linear, this diagram describes the behaviour of the tested cylinder during compressive loading. Due to the nature of the test performed as part of each experiment, the diagram simultaneously also describes the behaviour in uniaxial compression of the concrete from which the cylindrical specimens were manufactured, and it is easy to derive the ultimate strength of the tested concrete in uniaxial compression from the diagram.

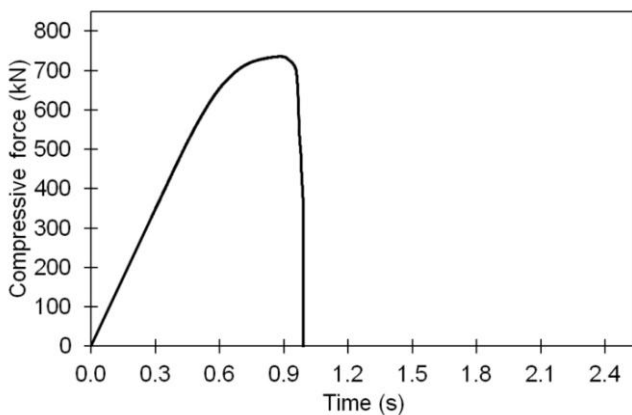


Fig. 2 Load-time diagram

During the compressive loading, each tested concrete cylinder first exhibited linearly elastic behavior, and then elasto-plastic behavior. From the moment when the maximum compressive force (i.e. the maximum compression load capacity of the concrete cylinder) was exceeded, the concrete began to show signs of compressive strain softening. In other words, deformation of the concrete cylinder began to increase at the same time as compressive force started decreasing. The compressive strain softening of the concrete began to assert

itself as a result of the damage to the concrete cylinder as the ultimate strength of the concrete in uniaxial compression was exceeded. The drop in compressive strength to zero as deformation increased was very rapid, which suggests that the concrete fractured in a brittle manner (see Fig. 2).

The maximum measured compressive force was 736.028 kN. The measured ultimate strength of the concrete in uniaxial compression was therefore approximately 42 MPa.

### III. NONLINEAR MATERIAL MODELS OF CONCRETE

Five types of nonlinear material model, which are implemented in LS-DYNA explicit finite element software ([17], [18]), were used for the purposes of this paper. Their brief description is given in the following subsections.

#### A. The Continuous Surface Cap Model

The Continuous Surface Cap material model ([19], [20]) is based on a yield surface which is described as a function of three stress invariants [21], [22]:

$$Y(I_1, J_2, J_3) = J_2 - \mathfrak{R}(J_3)^2 F_f^2(I_1) F_c(I_1, \kappa) \quad (1)$$

where  $I_1$  is the first invariant of the stress tensor,  $J_2$  and  $J_3$  are the invariants (second and third) of the deviatoric stress tensor,  $\mathfrak{R}(J_3)$  is the Rubin strength reduction factor and  $\kappa$  is the cap hardening parameter. The yield surface is composed of two parts, these being the shear failure surface  $F_f(I_1)$  and the hardening compaction surface  $F_c(I_1, \kappa)$ . The shear failure surface and hardening compaction surface are combined using a multiplicative formulation which allows their combination to be continuous and smooth at their intersection. The shear failure surface is defined as:

$$F_f(I_1) = \alpha - \lambda \exp^{-\beta I_1} + \theta I_1 \quad (2)$$

where  $\alpha$ ,  $\beta$ ,  $\lambda$ , and  $\theta$  are the material constants determined from the triaxial compression test data. The expression of the hardening compaction surface is given by:

$$F_c(I_1, \kappa) = 1 - \frac{(I_1 - L(\kappa))^2}{(X(\kappa) - L(\kappa))^2} \quad \text{for } I_1 > L(\kappa) \quad (3)$$

$$F_c(I_1, \kappa) = 1 \quad \text{for } I_1 \leq L(\kappa) \quad (4)$$

with

$$L(\kappa) = \kappa \quad \text{for } \kappa > \kappa_0 \quad (5)$$

$$L(\kappa) = \kappa_0 \quad \text{for } \kappa \leq \kappa_0 \quad (6)$$

$$X(\kappa) = L(\kappa) + R F_f(I_1) \quad (7)$$

where  $R$  is the cap aspect ratio.

The model includes the ability to generate parameters based on the uniaxial compressive strength, and allows the effect of strain rate, failure and different mechanico-physical properties in compression and tension to be taken into account.

#### B. The Winfrith Concrete Model

The Winfrith Concrete material model ([3], [23], [24]) is based on Ottosen's shear failure surface, and is defined as a

smearing crack and smeared rebar model. The Ottosen's shear failure surface is defined as [25]:

$$F(I_1, J_2, \cos 3\theta) = a \frac{J_2}{(f_c)^2} + \lambda \frac{\sqrt{J_2}}{f_c} + b \frac{I_1}{f_c} - 1 \quad (8)$$

with

$$\cos 3\theta = \frac{3\sqrt{3}}{2} \frac{J_3}{J_2^{3/2}} \quad (9)$$

$$\lambda = k_1 \cos \left[ \frac{1}{3} \cos^{-1}(k_2 \cos(3\theta)) \right] \text{ for } \cos 3\theta \geq 0 \quad (10)$$

$$\lambda = k_1 \cos \left[ \frac{\pi}{3} - \frac{1}{3} \cos^{-1}(-k_2 \cos(3\theta)) \right] \text{ for } \cos 3\theta \leq 0 \quad (11)$$

where  $I_1$  is the first invariant of the stress tensor,  $J_2$  and  $J_3$  are the invariants (second and third) of the deviatoric stress tensor,  $f_c$  is the unconfined (uniaxial) compressive strength,  $\theta$  is the lode angle and parameters  $a$ ,  $b$ ,  $k_1$ , and  $k_2$  are functions of the ratio of tensile strength to compressive strength ( $f_t/f_c$ ). Parameters  $a$ ,  $b$ ,  $k_1$ , and  $k_2$  are determined from the uniaxial, biaxial and triaxial compression tests.

The model allows the effect of strain rate, reinforcement and different mechanico-physical properties in compression and tension to be taken into account.

### C. The Damage Plastic Concrete Model

The Damage Plastic Concrete material model [26] is based on a yield surface described in Haigh-Westergaard coordinates, the flow rule, hardening law and evolution law, and is defined as a constitutive model based on the combination of damage mechanics and plasticity [27].

The model allows the effect of strain rate, failure and different mechanico-physical properties in compression and tension to be taken into account.

### D. The Karagozian & Case Concrete Model - Release 3

The Karagozian & Case Concrete material model - Release 3 ([28], [29]) is defined as a three-invariant model using three shear failure surfaces (initial yield surface, maximum shear failure surface and residual failure surface). These strength surfaces are independent and their formulation in a generalized form is given by [30]:

$$F_i(p) = a_{0i} + \frac{p}{a_{1i} + a_{2i}p} \quad (12)$$

where  $i$  stands for  $y$  (initial yield surface),  $m$  (maximum shear failure surface) or  $r$  (residual failure surface),  $a_{ji}$  ( $j = 0, 1, 2$ ) are parameters calibrated from the test data and  $p$  is the pressure, which is dependent on the first invariant of the stress tensor ( $p = -I_1/3$ ). The failure surface is interpolated between the maximum shear failure surface and either the initial yield surface or the residual failure surface:

$$F(I_1, J_2, J_3) = r(J_3)[\eta(\lambda)(F_m(p) - F_r(p)) + F_y(p)] \text{ for } \lambda \leq \lambda_m \quad (13)$$

$$F(I_1, J_2, J_3) = r(J_3)[\eta(\lambda)(F_m(p) - F_r(p)) + F_r(p)] \text{ for } \lambda > \lambda_m \quad (14)$$

where  $I_1$  is the first invariant of the stress tensor,  $J_2$  and  $J_3$  are the invariants (second and third) of the deviatoric stress tensor,  $\lambda$  is the modified effective plastic strain or the internal damage parameter,  $\eta(\lambda)$  is the function of the internal damage parameter  $\lambda$  and  $r(J_3)$  is the scale factor in the form of the William-Warnke equation [31].

The model includes the ability to generate parameters based exclusively on the uniaxial compressive strength, and allows the effect of strain rate, failure and different mechanico-physical properties in compression and tension to be taken into account.

### E. The Karagozian & Case Concrete Model

The Karagozian & Case Concrete material model is the original release of the Karagozian & Case Concrete Model - Release 3. The model allows the effect of strain rate, failure, reinforcement and different mechanico-physical properties in compression and tension to be taken into account.

## IV. NUMERICAL SIMULATIONS

### A. Description of the simulated uniaxial compression tests

In a real uniaxial compression test, a concrete cylinder is placed between the pressure plates of a test press. For the purposes of the numerical simulations in this paper, it was assumed that the friction between the surface of the cylinder base and the surface of the pressure plates is so great that it prevents any kind of horizontal displacement. This assumption enabled cylindrical specimen with crosswise-supported basal nodes to be modeled alone without the pressure plates. Schematically, this assumption can be represented in the form of a cylinder with fixed bases that allow vertical freedom of movement (see Fig. 3).

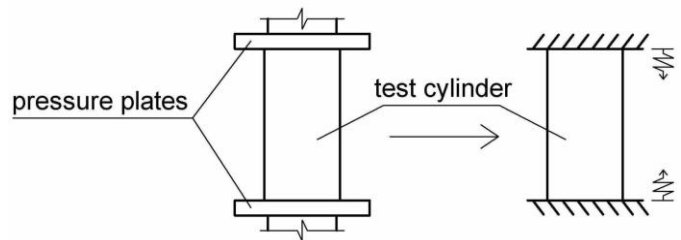


Fig. 3 Idealization of boundary conditions for the uniaxial compression test simulations

Within the numerical uniaxial compression test simulations, the cylinder was considered to be loaded via compression at a constant velocity from both sides. The vertical displacement of both bases of the cylinder over time thus grew linearly and evenly, during which the cylinder was loaded beyond its limits, and failed (see Fig. 4).

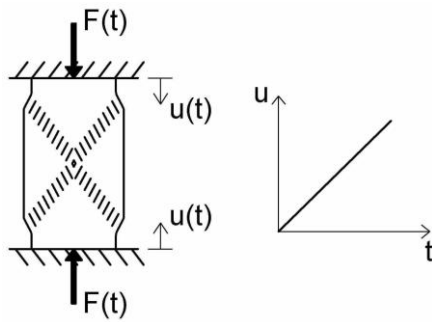


Fig. 4 Loading of the cylinder for the uniaxial compression test simulations

### B. Results of the numerical uniaxial compression test simulations, and their comparison with experimental results

The results of the numerical simulations performed in LS-DYNA software are depicted in a load-time diagram (see Fig. 5). It is clear from the diagram that during the compressive loading, the concrete cylinder first exhibited linearly elastic behavior and then elasto-plastic behavior for all of the nonlinear models of concrete used. From the moment when the maximum compressive force (i.e. the maximum compression load capacity of the concrete cylinder) was exceeded, the concrete in most of the nonlinear models began to show signs of compressive strain softening. In other words, deformation of the concrete cylinder began to increase at the same time as compressive force started decreasing. The compressive strain softening of the concrete began to assert itself as a result of the damage to the concrete cylinder as the ultimate strength of the concrete in uniaxial compression was exceeded.

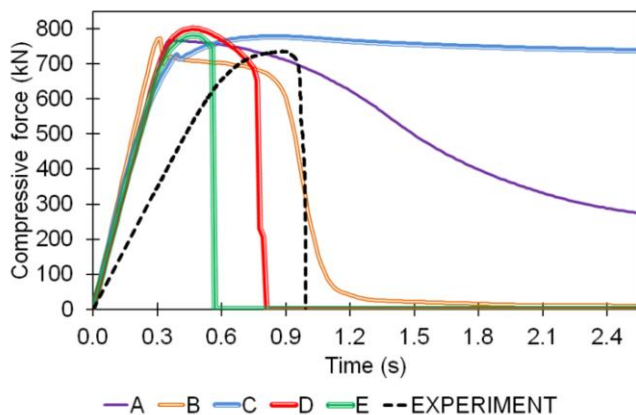


Fig. 5 Comparison of the calculations and the experimental results  
 Note: Curve A - The Continuous Surface Cap Model; Curve B - The Winfrith Concrete Model; Curve C - The Damage Plastic Concrete Model; Curve D - The Karagozian & Case Concrete Model - Release 3; Curve E - The Karagozian & Case Concrete Model.

Fig. 5 compares the finite element calculations and the experimental results. On the basis of this comparison it can be seen that the results of the numerical simulations demonstrate a good degree of agreement with the experimental results with regard to the maximum attained compressive force and to the behavior of concrete in uniaxial compression. Differences in the development of the compressive force over time between

the calculations and the experimental results are caused in particular by the partial incompatibility of the boundary conditions established for the numerical simulations with the boundary conditions used within the experiments. For this reason, the effect of boundary conditions on the results of the numerical simulations is dealt with in the next subsection.

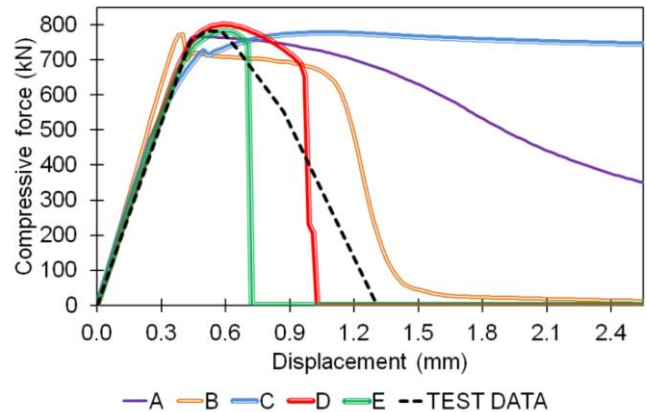


Fig. 6 Comparison of the calculations and the test data [32]

The load-displacement diagram in Fig. 6 compares the calculations and test data taken from [32]. The boundary conditions established for the numerical simulations in this paper correspond to the boundary conditions used within the experiments from which the test data were obtained. The results of the numerical simulations therefore demonstrate a good degree of agreement with the test data in terms of the evolution of compressive force versus displacement, and it is evident that the Karagozian & Case Concrete material models provide the best approximation of the test data (see Fig. 6). It follows that these nonlinear material models with the given parameter values best describe the behavior of the given concrete in uniaxial compression.

### C. Effect of boundary conditions on the results of the numerical simulations of uniaxial compression tests

The load-displacement diagram in Fig. 7 shows the results of the numerical uniaxial compression test simulations for different boundary conditions. Two types of curves are shown in this diagram. The dashed curves represent the calculations for the finite element model of the cylinder with crosswise-supported nodes used for one of its bases. The solid curves represent the calculations for the model of the cylinder with no supports. Nonlinear concrete models A - E are indicated in a manner corresponding to the note below Fig. 5. It is evident from the comparison of the calculations in Fig. 6 (calculations for the model of the cylinder with crosswise-supported bases) with the calculations in Fig. 7 that before the ultimate concrete strength in uniaxial compression is reached, the evolution of compressive force versus displacement is practically identical for all given boundary conditions. The calculations for the given boundary conditions differ only in terms of the post-peak compressive behavior of the concrete; in some cases they do not differ at all.

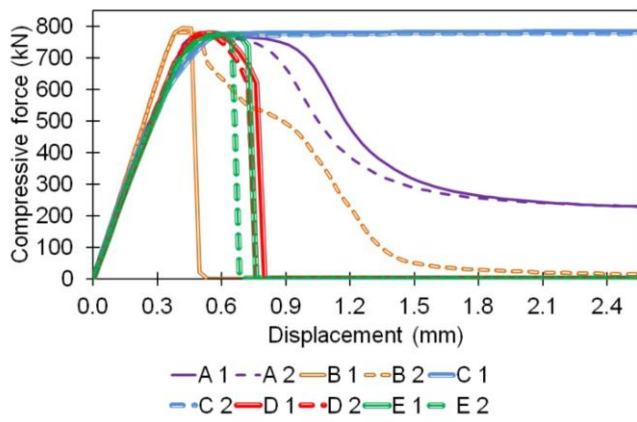


Fig. 7 Results of the numerical uniaxial compression test simulations for different boundary conditions

Fig. 8 shows a comparison between the results of the numerical simulations for different boundary conditions and the experimental results. In this figure, the solid curves represent the calculations for the model of the cylinder with crosswise-supported bases. The dashed curves represent the calculations for the finite element model of the cylinder between crosswise-supported plates whose material was modeled as steel. Nonlinear concrete models A - E are again indicated in a manner corresponding to the note below Fig. 5. It is clear from the load-time diagram in Fig. 8 that in the case of the cylinder held between plates, the maximum compressive force was reached later in time than in the case of the cylinder without plates for practically all of the nonlinear models used. The results for the cylinder held between plates therefore provide a better approximation of the experimental results, while the Winfrith Concrete material model provides the best approximation of the experimental data in terms of the evolution of compressive force over time before the ultimate concrete strength in uniaxial compression is reached.

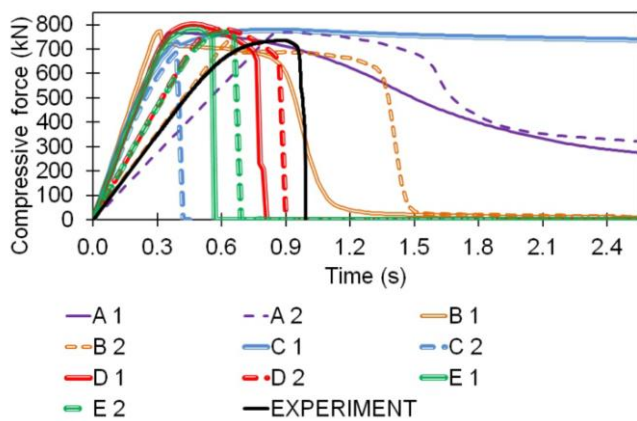


Fig. 8 Comparison of the calculations for different boundary conditions and the experimental results

*D. Description of the simulated triaxial compression tests*

In a real triaxial compression test, a concrete cylinder is placed between the pressure plates in the triaxial test chamber of a triaxial apparatus. For the numerical triaxial compression test simulations, the same assumptions as in the case of the

uniaxial compression test simulations (Fig. 3) were established in terms of boundary conditions (see Fig. 9).

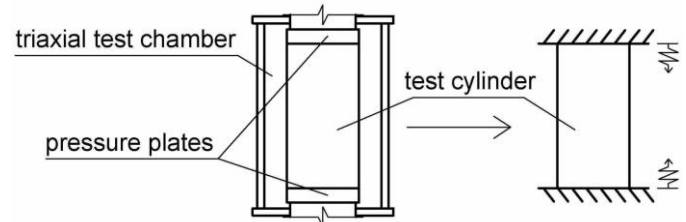


Fig. 9 Idealization of boundary conditions for the triaxial compression test simulations

Within the triaxial compression test simulations, the cylinder was considered to be loaded via compression at a constant velocity from both (top and bottom) sides and via constant pressure (confinement) over time from the side. The vertical displacement of both bases of the cylinder over time thus grew linearly and evenly, during which the cylinder was loaded beyond its limits, and failed (see Fig. 10).

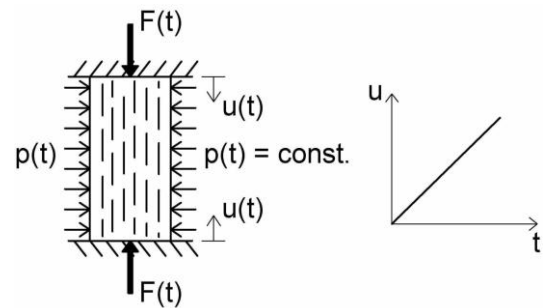


Fig. 10 Loading of the cylinder for the triaxial compression test simulations

*E. Results of the numerical triaxial compression test simulations, and their comparison with experimental data*

The results of the numerical triaxial compression test simulations for two levels of confinement (7 MPa and 20 MPa) are depicted in the load-displacement diagrams in Fig. 11 and Fig. 12. It is clear from the diagrams that during the compressive loading at both levels of confinement, the concrete cylinder first exhibited linearly elastic behavior and then elasto-plastic behavior for all of the nonlinear models of concrete used. It is also evident from the diagrams that the maximum compressive force (i.e. the maximum compression load capacity of the concrete cylinder) increased along with the increasing level of confinement for all of the nonlinear models used. Furthermore it is seen that in the case of both levels of confinement, the cylinder exhibited much more ductile post-peak compressive behavior than in the case of the cylinder without confinement (see Fig. 6) for most of the nonlinear material models used. Nonlinear concrete models A - E in Fig. 11 and Fig. 12 are indicated in a manner corresponding to the note below Fig. 5.

Fig. 11 and Fig. 12 also compare the calculations for the levels of confinement of 7 MPa and 20 MPa with the relevant test data taken from [32]. Since the boundary conditions

established for the numerical simulations in this paper correspond to the boundary conditions used within the experiments from which the test data were obtained, the results of the numerical simulations demonstrate a good degree of agreement with the test data in terms of the evolution of compressive force versus displacement before the ultimate concrete strength in triaxial compression is reached. This is also true with regard to the behavior of concrete in triaxial compression. It is evident from the figures that the Karagozian & Case Concrete material models provide the best approximation of the test data. Therefore, these nonlinear material models with the given parameter values best describe the behavior of the given concrete in triaxial compression.

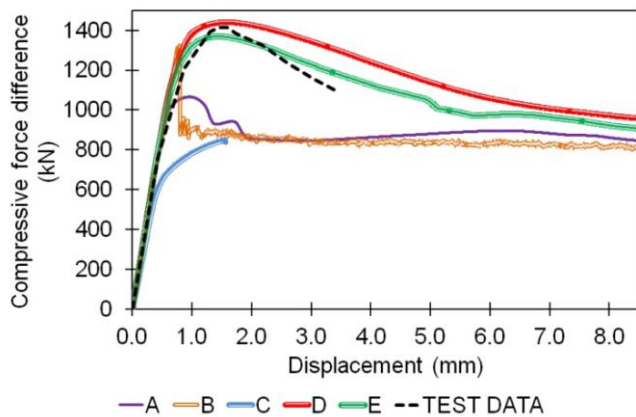


Fig. 11 Comparison of the calculations for the level of confinement of 7 MPa and the test data [32]

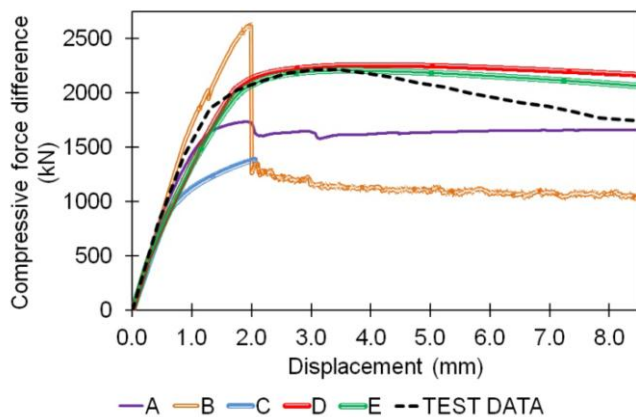


Fig. 12 Comparison of the calculations for the level of confinement of 20 MPa and the test data [32]

#### V. CONCLUSION

In this paper, the behavior of nonlinear concrete material models was validated by comparing the results of their calculations and obtained experimental data. The comparison showed that in some respects there was good agreement between the results obtained from the numerical simulations and the experimental results. This indicates that the parameter values of the individual nonlinear material models of concrete used were assigned appropriately for the numerical simulations. However, the results obtained for the Karagozian

& Case Concrete material models provided the best approximation of the experimental data, and therefore these nonlinear models of concrete with the given parameter values best described the behavior of the given concrete in uniaxial and triaxial compression.

In addition, the effect of boundary conditions on the results of the numerical simulations of uniaxial compression tests was studied. This study showed how the boundary conditions affected the behavior of a concrete cylinder in uniaxial compression as calculated within the numerical simulations, especially in terms of the evolution of compressive force over time.

#### REFERENCES

- [1] P. Hradil, J. Kala, and V. Salajka, "Analysis of roadside safety barrier using numerical model," *Safety and Reliability: Methodology and Applications - Proceedings of the European Safety and Reliability Conference, ESREL 2014*, pp. 29-32, Print ISBN 978-1-138-02681-0, eBook ISBN 978-1-315-73697-6.
- [2] J. Kala, P. Hradil, and M. Bajer, "Reinforced concrete wall under shear load – Experimental and nonlinear simulation," *International Journal of Mechanics*, 9, pp. 206-212, 2015, ISSN: 1998-4448. <http://www.scopus.com/inward/record.url?eid=2-s2.0-84934767684&partnerID=40&md5=d16fd43f45f8bb91e2829340435aa4d3>
- [3] B. J. Broadhouse and A. J. Neilson, "Modelling reinforced concrete structures in DYNA3D," *The DYNA3D user group conference*, London, September 1987.
- [4] P. Hradil and J. Kala, "Analysis of the shear failure of a reinforced concrete wall," *Applied Mechanics and Materials*, 621, pp. 124-129, 2014.
- [5] F. Hokes, J. Kala, and O. Krnavek, "Optimization as a Tool for the Inverse Identification of Parameters of Nonlinear Material Models," In: *Proceedings of the 9th International Conference on Continuum Mechanics (CM '15)*, 7-9 November 2015, Rome, Italy, A. Bulucea (Eds.), pp. 50-55, ISBN 978-1-61804-346-7, ISSN 2227-4359.
- [6] P. Hradil and J. Kala, "Nonlinear Behaviour of the Concrete Specimen under Shear load," In: *Proceedings of 3rd International Conference on Mathematical, Computational and Statistical Sciences (MCSS 15)*, pp. 248-253, Dubai, UAE, February 22-24, 2015, N. E. Mastorakis, A. Ding, M. V. Shitikova (Eds.), ISBN 978-1-61804-275-0, ISBN 978-1-61804-278-1 CD, ISSN 2227-4588.
- [7] J. Kala and M. Husek, "Useful Material Models of Concrete when High Speed Penetrating Fragments are Involved," In: *Proceedings of the 9th International Conference on Continuum Mechanics (CM '15)*, 7-9 November 2015, Rome, Italy, A. Bulucea (Eds.), pp. 190-193, ISBN 978-1-61804-346-7, ISSN 2227-4359.
- [8] P. Kral, J. Kala, and P. Hradil, "Validation of the Response of Concrete Nonlinear Material Models Subjected to Dynamic Loading," In: *Proceedings of the 9th International Conference on Continuum Mechanics (CM '15)*, 7-9 November 2015, Rome, Italy, A. Bulucea (Eds.), pp. 182-185, ISBN 978-1-61804-346-7, ISSN 2227-4359.
- [9] T. Zhan, Z. Wang, and J. Ning, "Failure behaviors of reinforced concrete beams subjected to high impact loading," *Engineering Failure Analysis*, October 2015, ISSN: 1350-6307.
- [10] M. Wu, Z. Chen, and C. Zhang, "Determining the impact behavior of concrete beams through experimental testing and meso-scale simulation: I. Drop-weight tests," *Engineering Fracture Mechanics*, Volume 135, February 2015, pp. 94-112, ISSN: 1350-6307.
- [11] Z. Kala, "Sensitivity and reliability analyses of lateral-torsional buckling resistance of steel beams," *Archives of Civil and Mechanical Engineering*, vol. 15, no. 4, pp. 1098-1107, 2015.
- [12] M. Yousufa, B. Uy, Z. Tao, A. Remennikov, and J. Y. R. Liew, "Impact behaviour of pre-compressed hollow and concrete filled mild and stainless steel columns," *Journal of Constructional Steel Research*, Volume 96, May 2014, pp. 54-68, ISSN: 0143-974X.
- [13] Z. Kala, J. Kala, M. Škaloud, and B. Teplý, "Sensitivity analysis of the effect of initial imperfections on the (i) ultimate load and (ii) fatigue

- behaviour of steel plate girders,” *Journal of Civil Engineering and Management*, vol. 11, no. 2, pp. 99–107, 2005.
- [14] M. Sadiq, X. Y. Zhu, and P. Rong, “Simulation analysis of impact tests of steel plate reinforced concrete and reinforced concrete slabs against aircraft impact and its validation with experimental results,” *Nuclear Engineering and Design*, Volume 273, 1 July 2014, pp. 653-667, ISSN: 0029-5493.
- [15] W. H. Dilger, R. Koch, and R. Kowalczyk, “Ductility of plain and confined concrete under different strain rates,” *ACI Journal*, January-February 1984.
- [16] F. Fedorik, J. Kala, A. Haapala, and M. Malaska, “Use of design optimization techniques in solving typical structural engineering related design optimization problems,” *Structural Engineering and Mechanics*, 55 (6), pp. 1121-1137. Techno-Press.  
<http://www.scopus.com/inward/record.url?eid=2-s2.0-84942878269&partnerID=40&md5=42da8772c33f8efafa8027f491414062>  
 DOI: 10.12989/sem.2015.55.6.1121
- [17] *LS-DYNA, Keyword User's Manual*, Livemore Software Technology Corporation, Livemore, California, 2015.
- [18] *LS-DYNA, Theory Manual*, Livemore Software Technology Corporation, Livemore, California, 2015.
- [19] Y. D. Murray, “Users manual for LS-DYNA concrete material model 159,” *Report No. FHWA-HRT-05-063*, Federal Highway Administration, 2007.
- [20] Y. D. Murray, A. Abu-Odeh, and R. Bligh, “Evaluation of concrete material model 159,” *Report No. FHWA-HRT-05-063*, 2006.
- [21] L. E. Schwer and Y. D. Murray, “A three invariant smooth cap model with mixed hardening,” *International Journal for Numerical and Analytical Methods in Geomechanics*, vol. 18, pp. 657-688, 1994.
- [22] I. S. Sandler, F. L. DiMaggio, and G. Y. Baladi, “Generalized cap model for geological materials,” *ASCE Journal of the Geotechnical Division*, vol. 102, pp. 683-699, 1976.
- [23] B. J. Broadhouse, “The Winfrith concrete model in Ls-dyna 3D,” *AEA technology*, Winfrith Technology Centre, 1995.
- [24] L. Schwer, “An Introduction to the Winfrith Concrete Model,” *Schwer Engineering & Consulting Services*, April 2010.
- [25] N. S. Ottosen, “A Failure Criterion for Concrete,” *Journal of the Engineering Mechanics Division*, Volume 103, Number 4, July/August, pp. 527-535, 1977.
- [26] P. Grassl, U. Nyström, R. Rempling, and K. Gylltoft, “A damage-plasticity model for the dynamic failure of concrete,” *8th International Conference on Structural Dynamics*, Leuven, Belgium, 2011.
- [27] P. Grassl and M. Jirasek, “Damage-plastic model for concrete failure,” *International Journal of Solids and Structures*, Volume 43, Issues 22-23, November 2006, pp. 7166-7196, ISSN: 0020-7683.
- [28] L. J. Malvar and D. Simons, “Concrete material modeling in explicit computations,” *Workshop on Recent Advances in Computational Structural Dynamics and High Performance Computing*, USAE Waterways Experiment Station, April 24-26 1996.
- [29] L. J. Malvar, J. E. Crawford, J. W. Wesevich, and D. Simons, “A plasticity concrete material model for Dyna3d,” *International Journal of Impact*, vol. 19, Nos. 9-10, pp. 847-873, Elsevier, 1997.
- [30] W. Youcai, J. E. Crawford, and J. M. Magallanes, “Performance of LS-DYNA Concrete Constitutive Models,” *12th International LS-DYNA Users Conference*, Detroit, 2012.
- [31] W. F. Chen and D. J. Han, *Plasticity for structural engineers*. Springer-Verlag, New York, 1988.
- [32] S. Joy and R. Moxley, “Material characterization, WSMR-5 3/4-inch concrete,” *Report to the Defense Special Weapons Agency*, USAE Waterways Experiment Station, Vicksburg, MS, 1993 (limited distribution).